Buildings Integrated Phase Change Materials: Modelling and Validation of a Novel Tool for the Energy Performance Analysis

Giovanni Avagliano – University of Naples Federico II – g.avagliano12@gmail.com
Annamaria Buonomano – University of Naples Federico II – annamaria.buonomano@unina.it
Maurizio Cellura – University of Palermo – maurizio.cellura@unipa.it
Vasken Dermardiros – Concordia University – vdermardiros@gmail.com
Francesco Guarino – University of Palermo – francesco.guarino@unipa.it
Adolfo Palombo – University of Naples Federico II – adolfo.palombo@unina.it

Abstract

In this paper a novel dynamic energy performance simulation model for the Phase Change Materials (PCM) analysis is presented. The model is implemented in a suitable computer code, written in MatLab and called DETECt, for complete building energy analyses. In the presented model, the "effective specific heat" method is implemented. Here, the specific heat of each PCM layer changes as a function of the system phase and temperature in both melting and freezing processes. A model validation is carried out by comparing numerical results vs. measurements obtained at Solar Laboratory of Concordia University (Montreal, Canada). The simulation model allows exploring the potential of PCMs to increase the thermal inertia of building envelopes and to assess the effects/ weight of several design parameters (e.g. PCMs melting temperature, etc.) on the building heating and cooling energy demand and on the related thermal comfort. In order to show the potentiality of the presented simulation model, suitable case studies referred to residential and office buildings, to three different weather conditions and to two alternative PCM layouts in the building envelope, are developed.

1. Introduction

Recently, the research of innovative solutions aimed at improving the energy efficiency and comfort of buildings, has become increasingly significant. Among the available techniques, the integration in the building envelope of Phase Change Materials (PCMs) can be considered (Kuznik et al., 2011). Basically, through such materials the thermal inertia of the building envelope can be increased by exploiting the latent heat stored in PCM during its melting process and by taking advantage of the latent heat of solid and liquid transformation. Thus, by the integration of PCM in the building envelope, the storage and release of thermal energy occurring during the phase change can effectively reduce heating/ cooling consumptions and increase thermal comfort (Dutil et al., 2014). In fact, the decrease and delay of the thermal loads implies a reduced fluctuation of the indoor air temperature with the enhancement of the building comfort (to avoid system overheating by dissipating or recovering the stored heat during late/night hours). Nevertheless, the proper exploitation of the latent heat stored in PCM is highly influenced by the building usage (Buonomano et al., 2016a). In addition, the use of PCMs in buildings also implies some criticisms such as: still high initial costs and some design and operating difficulties due to the variation of specific heat, thermal conductivity, and density during the phase change process (Liu et al., 2016).

In order to assess the potentiality of the building integration of PCMs, a number of computer tools for energy performance analyses of PCMs have recently been developed (Dutil et al., 2014). However, the knowledge of the thermodynamics properties of PCMs and phenomena governing their variation is crucial to select the suitable materials for the specific building and to model the system for the energy performance assessment. In case of conduction dominated phase change, e.g.,

microencapsulated PCMs (Kuznik et al., 2011), in literature the heat transfer phenomenon is modelled by means of both the apparent specific capacity and the enthalpy method, which can alternatively be used as a function of the available thermodynamics properties and the selected methodology (Al-Saadi and Zhai, 2015; Tittelein et al., 2015). Despite of their capability in predicting the thermal and energy behaviour of PCMs in buildings, different models based on these methods are available in literature (Kuznik et al., 2011; Dutil et al., 2014). Nevertheless, for the PCM characterization (such as the assessment of PCMs specific heat, c_P) the most widely adopted technique consists in the use of a Differential Scanning Calorimeter (DSC-method) (Dutil et al., 2014; Tittelein et al., 2015), together with the T-history method (Tittelein et al., 2015). Today, the measurement of the PCMs thermodynamics properties is an open problem for researchers and manufacturers due to several issues related, for example, to the mechanical confinement, chemical interaction, different enthalpy of melting and freezing, incomplete melting and freezing, nucleation process, measurement conditions (sample mass, heating and cooling rates), etc. vs. real ones (Kuznik et al., 2011). Therefore, review studies on this topic highlight the need of improved thermal characterization procedures (Dutil et al., 2014). Such procedures are also necessary for the proper design of effective PCMs for building applications, carried out through suitable building dynamic simulation modelling.

In this framework, the authors carried out the characterization of a commercially available PCM wallboard by calculating the thermodynamic PCMs properties from available experimental data. The obtained set of measurements (collected in diverse conditions) was used in order to tune the c_P profiles, variable as a function of the occurring temperature. Such novel profiles are implemented in a dynamic building energy performance simulation tool written in MatLab (DETECt 2.2) (Buonomano and Palombo, 2014), for whole building energy performance analyses. Finally, in order to show the potential of such tool, the authors developed a case study on a building integrating PCMs, located in a different weather zone.

2. Simulation Model

The simulation model used for the analysis of the PCM building integration is based on the finite difference method, assuming a one-dimensional thermal domain. By such model, called DETECt 2.2 and validated through a code-to-code validation procedure (Buonomano, 2016), the assessment of temperatures and humidity dynamics, as well as of heating and cooling loads and demands, can be carried out (Buonomano and Palombo, 2014).

The physical building model consists in a resistive-capacitive (RC) thermal network obtained by distributed parameters (Tsilingiris, 2006). Fig. 1 shows a sketch of the modelled *RC* thermal network for one thermal zone.

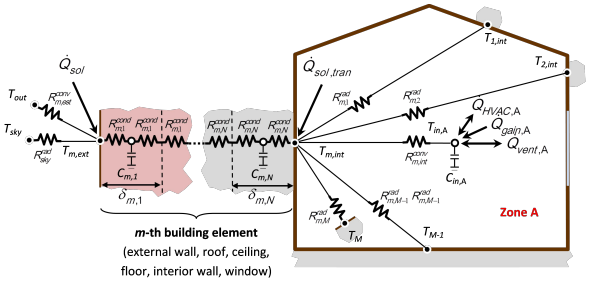

Fig. 1 – Simulation model: RC thermal network

The following model simplifications are considered: i) the indoor air of each thermal zone is considered as uniform and modelled as a single indoor air temperature node; ii) the building envelope is subdivided into M multi-layer elements (a high order *RC* thermal network); iii) each m-th multi-layer building element of a single zone is subdivided in N sub-layers, where thermal masses and conductivities are uniformly discretised; iv) $N+2$ capacitive and surface nodes are considered for each m-th envelope component; v) each PCM node is characterized by a dynamic variation of the heat capacity, dependent on:

- the temperature of the considered element;
- phase transition (melting/solidification).

In each (-th time step and for each n-th capacitive node of the m-th element, the differential equation describing the energy rate of change of each temperature node of the building envelope is:

$$C_{m,n}\frac{dT_{m,n}}{dt} = \sum_{j=n-1}^{n+1}\frac{T_{m,j} - T_{m,n}}{R_{m,j}^{eq}} \qquad (1)$$

where $R^{eq}_{m,j}$ is the sum of the halves sub-layers thermal resistances $R^{cond}_{m,j}$ linking the *n*-th node to their neighbours (Fig. 1). For non-capacitive outer (n = 0) and inner (n = N+1) surface boundary nodes, the heat transfer is calculated by:

$$\sum_{j=n-1}^{n+1} \frac{T_{m,j} - T_{m,n}}{R^{cv}_{m,j}} + \dot{Q}_{m,n} = 0 \qquad (2)$$

where $R^{cv}_{m,j}$ is either a convective (external $R^{conv}_{m,0}$ or internal $R^{conv}_{m,N+1}$ non-capacitive nodes) or a conductive resistance ($R^{cond}_{m,n}$), depending on the side layer of the considered node (Fig. 1). $\dot{Q}_{m,n}$ is a forcing function including incident solar and long-wave radiation exchange acting on outer and inner surfaces of thermal zone (Buonomano, 2016).

The differential equations on the thermal network nodes must be solved simultaneously with the system of Equations (1) and (2). The sensible energy rate of change of indoor air masses can be calculated as:

$$C_{in}\frac{dT_{in}}{dt} = \sum_{m=1}^{M} \frac{T_{m,N} - T_{in}}{R^{conv}_{m,N+1}} + \dot{Q}_{gain} + \dot{Q}_{vent} \pm \dot{Q}_{ac} \quad (3)$$

where $\dot{Q}_{gain}$ is the internal load due to occupants, lights, and equipment; $\dot{Q}_{vent}$ is the ventilation thermal load; $\dot{Q}_{hc}$ is the sensible heat to be supplied to or removed from the thermal zone by an ideal heating and cooling system. Additional details are reported in (Buonomano and Palombo, 2014).

The modelling approach is suitable for the assessment of the phenomenon of phase change, taken into account by using the effective heat capacity method (Tittelein et al., 2015). By such technique, a temperature dependent thermal capacitance c_P is assumed, during both the melting and solidification processes (i.e. to take into account the hysteresis phenomenon typical for paraffin materials). It is worth noting that the whole building model is partially implicit, and the effective heat capacity of each node (by varying the thermal capacitance in Equation (1) as a function of the time) is calculated at the previous time step (Kuznik et al., 2015; Buonomano et al., 2016b). In order to model the PCM building integration, the effective heat capacity curve of the PCM, together with the conductivity one, as suggested by literature (Kuznik et al., 2008), was first implemented in the model and then calibrated as a function of the available experimental data. Such inverse approach was adopted to enhance the reliability of PCM specific heat during phase change processes.

3. Experimental analysis

The PCM behaviour in the indoor environment was assessed through experimentation (Guarino et al., 2015; Guarino et al., 2017). A small test room with a large window was fitted with PCM modules on the (opposing) back wall. The test room (Fig. 2) has interior dimensions: 2.80 m width × 1.30 m depth × 2.44 m height, with an overall conductance of 0.2 W/(m² K). The window is double-glazed (2 m × 2 m, U = 1.7 W/(m² K), visible transmittance of 0.616, SHGC = 0.262) with 6 mm low-e glass and a 12 mm gap filled with Argon.

The PCM used in the experiment is a commercially-available PCM wallboard, described in Kuznik et al. (2008). It is a mixture of 40 % ethylene-based polymer and 60 % paraffin wax, with a density of 900 kg/m³. The panels (5.2 mm thick, 1000 mm wide and 1198 mm long) are encapsulated with 100 μm aluminum layer on both sides. The latent heat is 70 kJ/kg, with a melting point peaking at 21.7 °C. 20 PCM sheets were installed on the back wall of the test room.

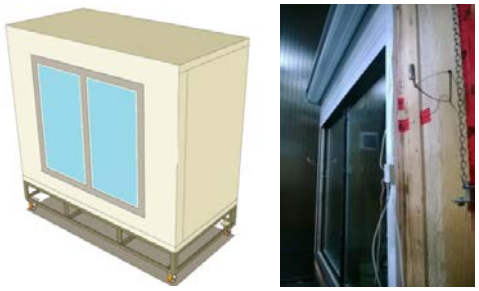

Fig. 2 – Schematic and front view of the test room

They were divided in four groups, each with 5 layers of PCM panels, for a total of roughly 100 kg.

The experimental setup took place in the Solar Simulator Environmental Chamber facility at Concordia University (Montreal, Canada).

Basically, it is featured by two solar simulators and a climatic chamber in which temperatures and relative humidity can be varied between -40 °C and +50 °C and 20 % and 95 %, respectively. The test room, placed inside the climatic chamber was subjected to radiation emitted by a full-scale solar simulator (Fig. 3a). In combination with glass filters, 6 metal halide lamps provide a spectral distribution close to natural sunlight, fulfilling the EN12975: 2006 and ISO 9806-1:1994 specifications.

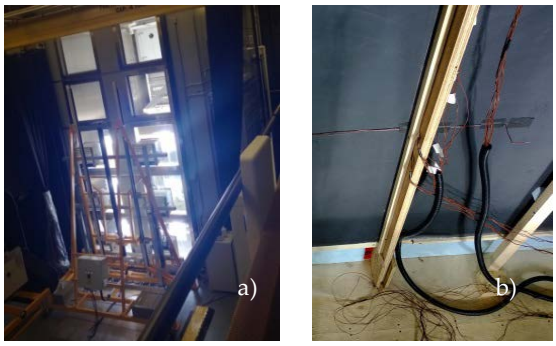

Fig. 3 – a) Solar simulator – b) Back wall PCM panels

Test room temperatures were monitored by using Type T thermocouples placed: in each PCM inter-layer interface; on the back wall (at different heights and at 5 cm distance from the PCM panels, Fig. 3b); on the remaining room interior surfaces. Air temperature in the test room was monitored at 4 different heights.

The carried out tests can be summarized as follows:

Test 1: Duration: 75 hours. Environmental chamber temperature: 16 °C. Test room heating obtained with a 350 W fan-coil for 21 hours (free-floating temperature for the remaining time);

Test 2: Duration: 75 hours. Quasi-sinusoidal air temperature profile in the environmental chamber with a peak of 20 °C (every day) and a minimum of 10 °C (first day) and 6° C (second and third day), the average solar radiation was 500 W/m² (9:30 am - 1:00 pm for the first day and 9:30 am - 12:30 am for the second and the third day).

For both tests the measured data were logged every 3 minutes, by averaging readings performed every 30 seconds).

4. Model validation

The model validation was performed by simulating both the experimental tests described in the previous section. Specifically, two suitable case studies were modelled in order to faithfully repeat all the above-mentioned boundary conditions. Several simplification assumptions were taken into account in the developed simulation code, such as: i) a single PCM layer (suitably divided into 5 capacitive nodes) was considered for both tests; ii) mono-dimensional heat flux is considered in the modelled PCM; iii) in Test 1 the fan coil outlet air interacts with the PCM wall only by natural convection heat transfer (e.g. considered as convective input (as $\dot{Q}_{hc}$) in Equation (3); iv) in Test 2 the incident radiation on the PCM wall is considered uniform and perpendicular to the surface (whereas a difference ranging from 430 to 590 W/m² was effectively detected on the radiated surface).

Initially, the PCM melting and solidification c_P profiles were considered equal to those suggested in Kuznik et al. (2008). Nevertheless, the curve taken from publication was not suitable for the all the simulated tests (numerical results did not agree with all the experimental ones). Thus, the authors performed a subsequent model refinement, where the PCM c_P was iteratively obtained as a function of the reduction to the minimum of the deviation between the temperature $T_{k,i}$ (of the *k-th* node in the *i-th* time step) measured in the experimental tests and the one calculated by the simulation model. It is worth noting that convective and radiative external coefficients were suitably tuned in order to replicate the external boundary conditions occurring in the test chamber. By following this approach, new $c_P(t)$ curves, for solidification and melting were shaped. The resulting hysteresis is very slight, different from the majority of publications, but according to few authors as reported in Dutil et al. (2014). In fact, a remarkable presence of hysteresis (as the one of the first $c_P(t)$ curves) effectively created modelling inaccuracies in continuous simulated charging and discharging processes (as in Test 2). This might be ascribed to the dependence of the thermal behaviour on the history of heat loading, the heating rate, and on

incomplete melting/solidification (Dutil et al., 2014).

By taking into account the new curves, a comparison between experimental and model temperatures for the outermost PCM layer (Node 1), the innermost one (Node 5) and test cell indoor air is reported and showed in Fig. 4 and 5 for Test 1 and Test 2, respectively. A good agreement between measurements and numerical results is detected in both cases.

Such achievement is evident by observing also Fig. 6 and 7, depicting the time histories of the detected errors between experimental and simulation results, for all PCM and indoor air temperature nodes. Except for few brief time steps, model errors are always lower than ± 0.7 °C.

Note that, such errors are probably due to some uncertainties in the system modelling, as well as in measurements operations, mainly due to several occurrences, as: i) absence of radiation shading of the thermocouples for the measurement of the test chamber air temperature; ii) lack of uniform vertical temperature profile especially for Test 2; iii) conduction defect between the 5 overlapping PCM layers mainly due to the presence of the thermocouples (thin air-gap among PCM panels, simulated by slightly reducing their conductivity).

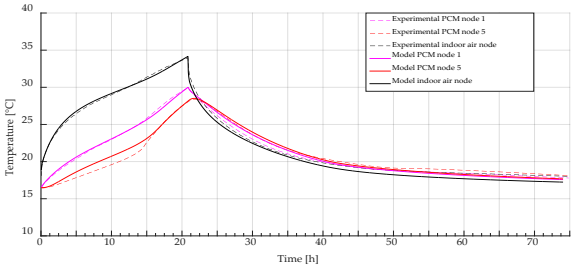

Fig. 4 – Test 1: experimental data vs. model result

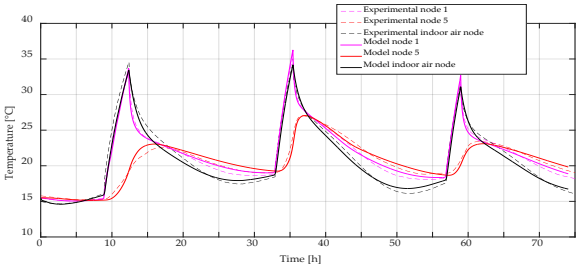

Fig. 5 – Test 2: experimental data vs. model result

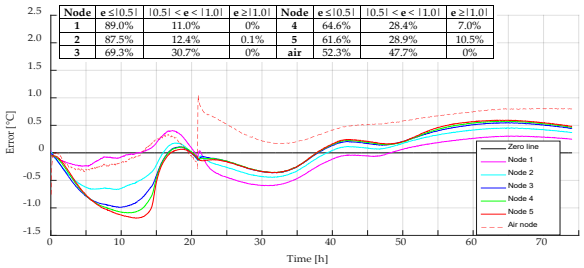

Node	e ≤ |0.5|	|0.5| < e < |1.0|	e ≥ |1.0|	Node	e ≤ |0.5|	|0.5| < e < |1.0|	e ≥ |1.0|
1	89.0%	11.0%	0%	4	64.6%	28.4%	7.0%
2	87.5%	12.4%	0.1%	5	61.6%	28.9%	10.5%
3	69.3%	30.7%	0%	air	52.3%	47.7%	0%

Fig. 6 – Test 1: error time history

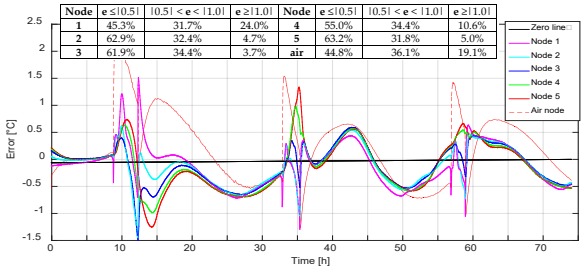

Node	e ≤ |0.5|	|0.5| < e < |1.0|	e ≥ |1.0|	Node	e ≤ |0.5|	|0.5| < e < |1.0|	e ≥ |1.0|
1	45.3%	31.7%	24.0%	4	55.0%	34.4%	10.6%
2	62.9%	32.4%	4.7%	5	63.2%	31.8%	5.0%
3	61.9%	34.4%	3.7%	air	44.8%	36.1%	19.1%

Fig. 7 – Test 2: error time history

5. Case Study

A suitable case study was developed in order to show the potentiality of the presented simulation model as well as the feasibility of PCM integration in interior walls (of external building rooms subjected to solar gains) toward the reduction of energy consumption and indoor air temperature fluctuations. For such analysis, an example of building integration of PCM was considered for a dwelling and an office building located in Naples, Palermo, and Montreal, calculating the related energy savings and the avoided CO_2. Specifically, a sample 8.0 × 6.0 m rectangular shaped lightweight building (with East-west oriented longitudinal axis), 3.0 m height, was modelled. The U-values of vertical walls, roof, and windows are respectively 0.49, 0.30, and 1.70 W/(m² K). A window SHGC of 0.262 is considered. More details are reported in Buonomano and Palombo (2014). The air flow rate for residential and office use is 0.5 and 1.2 Vol/h. A night free cooling ventilation strategy was also taken into account (2.0 Vol/h) if the outdoor air temperature is lower than the indoor one. Dynamic simulations were performed for one year by using Meteonorm weather data. The HVAC system is modelled by an electric air-to-water chiller/heat pump (heating and cooling COP = 3.5 and 3.0),

necessary to maintain the indoor air temperature between 20 °C and 26 °C. The system operation was scheduled as reported in Table 1. As initial investigation, the PCM panels were integrated on the East and West walls and on the roof only. Two different layouts were simulated, where PCM panels were integrated internally and externally to the building envelope.

Table 1 – Climatic zones, climatic indexes, and system scheduling

Weather zone	HDD Kd	CDD Kd	ISR kWh/m²y	Use	Heating Months (hours)	Cooling Months (hours)
Montreal	4567	297	1350	House	15/9-31/3 (0-24)	1/6-15/9 (11-18)
				Office	(8-20)	(8-20)
Naples	1479	499	1470	House	15/11-31/3 (7-10, 14-21)	1/6-30/9 (11-18)
				Office	(8-20)	(8-20)
Palermo	760	987	1664	House	1/12-31/3 (7-10, 14-21)	1/6-30/9 (11-18)
				Office	(8-20)	(8-20)

5.1 Results and Discussion

The monthly results for Naples are reported in Fig. 8 and 9, where the electricity demand of the chiller/heat pump is reported as a function of the different investigated system layouts. For residential applications (Fig. 8), the best configuration was reached by integrating the PCM externally to the building envelope. Simulations show that the overall summer cooling energy savings are maximized by boosting the PCM charge/discharge effect through a night free cooling ventilation. It is also worth noting that the PCM also causes a lower heating demand during the colder winter months. This is due to the heat required by the PCM charge (energy storage) basically obtained by an increase of the HVAC system demand vs. the reference case (no PCM). Such heat is dissipated during the time interval in which the heat pump is switched off (10:00 - 14:00). For office use (Fig. 9), the potential of a night free cooling strategy is higher vs. that observed for the residential use. In fact, in the office, during night hours, the absence of internal heat gains allows the PCM to complete a charge/discharge cycle. For office use, by adopting PCM a small winter saving is achieved because of the continuous HVAC system running from 08:00 to 20:00. Here, energy saving is achieved by exploiting the free solar heat stored by PCM during the winter sunny days. A similar behaviour is observed for Palermo.

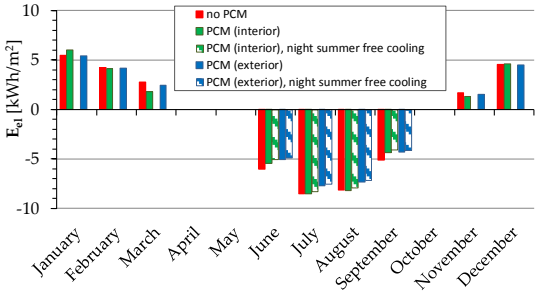

Fig. 8 – Residential building in Naples: monthly results

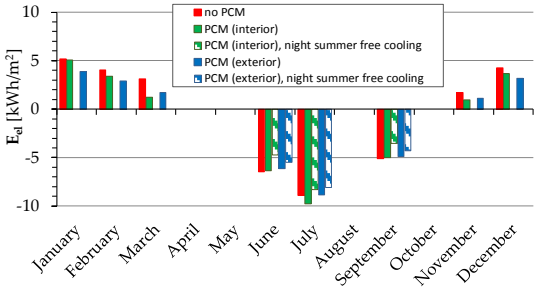

Fig. 9 – Office building in Naples: monthly results

The opposite result is achieved in winter in Montreal, where an increase of the heating demand is obtained by adopting PCM. For this climate zone, in Fig. 10 the time histories of the office indoor air temperature (Tin) and sensible heating load (Qac) are reported for the two PCM layouts, as well as in case of no PCM, for two winter sample days (January 5 and 6). Note that, on the second day (Saturday) the office in closed (the HVAC system is switched off). Whereas during the daytime when the HVAC system is switched on, the required indoor air temperature setpoint (26 °C) is always reached, in the nighttime a free-floating air temperature occurs. Due to the use of PCM, the minimum indoor air temperature decrease is obtained in case of interior PCM position, as expected (higher thermal comfort). Concerning the corresponding heating load (shown in Fig. 10 by averaging the predicted heating energy every hour), it is clearly visible that the lowest peak is obtained by placing the PCM on the interior position in the envelope (because of the higher indoor air temperature occurring at the start of the

HVAC system). As a result, the corresponding reduction of the heating peak load (occurring at the HVAC running start) is counterbalanced by an increase of the heating demand obtained during daytime (in Fig. 10 the green virtual area is larger than the other ones). In Fig. 11 for four summer sample days (July 13-16), the time histories of the indoor surface temperature of the West-building wall (with PCM), as well as the outdoor air temperature, are reported for the residential building use. Here, due to the PCM use, the obtained surface temperature peaks are attenuated and delayed vs. those related to the reference case without PCM, highlighting the effects due to the stored heat, delivered toward the indoor zone during nighttime. Note that a complete PCM charge/discharge cycle occurs.

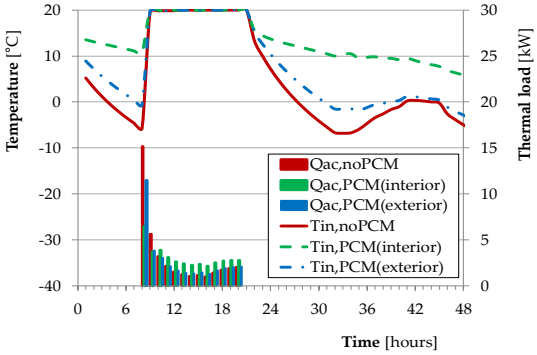

Fig. 10 – Two winter sample days in Montreal: office temperatures and loads

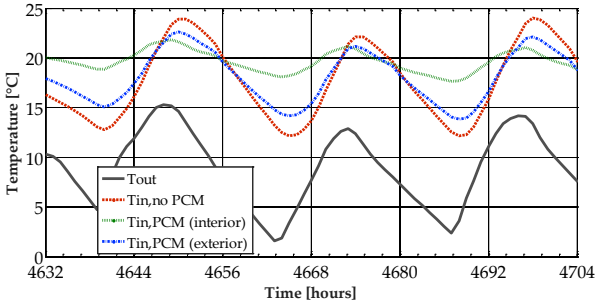

Fig. 11 - Four summer sample days in Montreal: outdoor air and interior surfaces temperatures for the residential building

In Fig. 12 for three winter sample days in Palermo (March 5-7) the time histories of the indoor air temperature with and without PCM, as well as the outdoor air temperature, are reported for the residential building. As expected the air temperatures approaching the comfort requirement occur especially in case of interior PCM positioning.

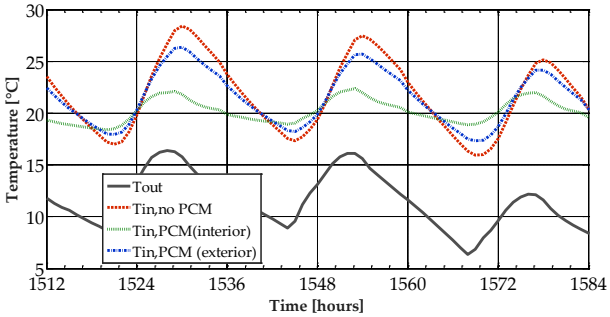

Fig. 1 – Free floating for three winter sample days in Palermo: outdoor and indoor air for the residential building

The obtained overall yearly results are reported in Table 2 and in Table 3. Here, the electricity demand of the chiller/heat pump of the traditional building (no PCM) as well as the achieved energy savings obtained by the PCM adoption are reported for all the investigated weather zones and system layouts. In the same tables the avoided CO_2 and the economic operative savings are also shown. For both the heating and cooling requirements interesting electricity savings are obtained (except for the heating demand in Montreal). For the standard system and the best system layout (exteriorly placed PCM) the overall energy savings range from 12 % to 15 %, whereas the avoided CO_2 from 21 to 42 kg/y (Table 2).

Table 2 – Yearly results for office use (standard)

Weather zone	Without PCM			With PCM					
	$E_{el,heat}$	$E_{el,cool}$	$E_{el,tot}$	PCM position	$\Delta E_{el,heat}$	$\Delta E_{el,cool}$	$\Delta E_{el,tot}$	ΔCO_2	ΔC
	$kWh_{el}/(m^2y)$				kWh_{el}/m^2y (%)			kg/y	€/y
Montreal	25.3	3.5	28.8	in	3.3 (+12.9)	-0.6 (-17.9)	2.6 (+9.2)	23.6	4.4
				out	-3.0 (-12.0)	-0.3 (-9.3)	-3.4 (-11.7)	-30.0	-16.7
Naples	5.2	6.8	12.1	in	-1.1 (-21.9)	0.2 (+3.1)	-0.9 (-7.7)	-21.8	-6.7
				out	-1.6 (-30.1)	-0.2 (-3.0)	-1.8 (-14.8)	-41.6	-12.8
Palermo	2.4	7.8	10.2	in	-1.8 (-75.8)	0.7 (+9.3)	-1.1 (-10.6)	-25.0	-7.7
				out	-1.3 (-55.6)	0.0 (+0.1)	-1.3 (-12.9)	-30.5	-9.4

Table 3 – Yearly results for office use (summer night ventilation)

Weather zone	Without PCM			With PCM					
	$E_{el,heat}$	$E_{el,cool}$	$E_{el,tot}$	PCM	$\Delta E_{el,heat}$	$\Delta E_{el,cool}$	$\Delta E_{el,tot}$	ΔCO_2	ΔC
	$kWh_{el}/(m^2 y)$			position	kWh_{el}/m^2y (%)			kg/y	€/y
Montreal CF_{CO2} = 0.186 [kg/kWh]	As in Table 2			in	As in Table 2	-1.7 (-48.1)	1.6 (+5.5)	14.3	2.6
				out		-0.7 (-21.5)	-3.8 (-13.1)	-33.8	-18.8
Naples CF_{CO2} = 0.486 [kg/kWh]				in		-1.3 (-19.3)	-2.5 (-20.4)	-57.5	-17.7
				out		-0.9 (-13.1)	-2.5 (-20.5)	-57.7	-17.8
Palermo CF_{CO2} = 0.486 [kg/kWh]	CF_{CO2} = national CO_2 conversion factor			in		-0.5 (-6.2)	-2.3 (-22.4)	-53.1	-16.4
				out		-0.6 (-8.3)	-2.0 (-19.4)	-45.9	-14.2

By the night free cooling ventilation strategy and for the same system layout, the overall energy savings range from 13 % to 21 % and the avoided CO_2 from 34 to 58 kg/y (Table 3). For all the investigated system configurations, the operating economic savings are still too low to balance the current initial PCM cost for acceptable paybacks.

6. Conclusions

The paper presents a validation procedure of a mathematical model (DETECt 2.2) for building simulation analyses involving the use of PCM wallboards. For the model validation procedure and the PCM characterization, measurements obtained by using PCM integrated in the back wall of a small test-cell under controlled conditions were used. The obtained numerical modelling is in good agreement with experimental data obtained during different tests (i.e. one charging cycle by a convective heating system and three charging cycles by solar irradiation). The tool allows the simulation of different scenarios (e.g., different PCM configurations, variable weather conditions, etc.), and the performance of parametric and sensitivity analyses to optimize the PCM building integration.

A case study analysis, carried out for a residential and an office building in three weather zones, shows the crucial influence of the building use (e.g., occupancy schedules, internal gains) on the exploitation of the latent heat stored in PCM layers. Finally, interesting design criteria for the development and adoption of building integrated PCMs are provided. Further analyses will be performed to investigate the relationships among PCM properties (e.g., peak melting temperature, melting range, etc.).

Nomenclature

Symbols

C	thermal capacitance *(J/K)*
$\dot{Q}$	thermal load *(W)*
R	thermal resistance *(K/W)*
T	temperature *(K)*

Subscripts/Superscripts

ac	HVCAC system
in	indoor air
out	outdoor air

References

Al-Saadi, S.N., Z. Zhai. 2015. "Systematic evaluation of mathematical methods and numerical schemes for modeling PCM-enhanced building enclosure". *Energy and Buildings* 92: 374-388. doi: 10.1016/j.enbuild.2015.01.044.

Buonomano, A. 2016. "Code-to-Code Validation and Application of a Dynamic Simulation Tool for the Building Energy Performance Analysis". *Energies* 9(4): 301. doi:10.3390/en9040301.

Buonomano, A., G. De Luca, U. Montanaro, A. Palombo. 2016a. "Innovative technologies for NZEBs: An energy and economic analysis tool and a case study of a non-residential building for the Mediterranean climate". *Energy and Buildings* 121: 318-343. doi: 10.1016/j.enbuild.2015.08.037.

Buonomano, A., U. Montanaro, A. Palombo, S. Santini. 2016b. "Dynamic building energy performance analysis: A new adaptive control strategy for stringent thermohygrometric indoor air requirements". *Applied Energy* 163: 361-386. doi: 10.1016/j.apenergy.2015.10.182.

Buonomano, A., A. Palombo. 2014. "Building energy performance analysis by an in-house developed dynamic simulation code: An investigation for different case studies". *Applied Energy* 113: 788-807. doi:10.1016/j.apenergy.2013.08.004.

Dutil, Y., D. Rousse, S. Lassue, L. Zalewski, A. Joulin, J. Virgone, F. Kuznik, K. Johannes, J.P. Dumas, J.P. Bédécarrats, A. Castell, L.F. Cabeza. 2014. "Modeling phase change materials behavior in building applications: Comments on material characterization and model validation". *Renewable Energy* 61: 132-135. doi: 10.1016/j.renene.2012.10.027.

Guarino, F., A. Athienitis, M. Cellura, D. Bastien. 2017. "PCM ther-mal storage design in buildings: Experimental studies and applications to solaria in cold cli-mates". *Applied Energy* 185: 95-106. doi: 10.1016/j.apenergy.2016.10.046.

Guarino, F., V. Dermardiros, Y. Chen, J. Rao, A. Athienitis, M. Cellura, M. Mistretta. 2015. "PCM Thermal Energy Storage in Buildings: Experimental Study and Applications". *Energy Procedia* 70: 219-228. doi: 10.1016/j.egypro.2015.02.118.

Kuznik, F., J.P. Arzamendia Lopez, D. Baillis, K. Johannes. 2015. "Phase change material wall optimization for heating using metamodeling". *Energy and Buildings* 106: 216-224. doi: 10.1016/j.enbuild.2015.06.021.

Kuznik, F., D. David, K. Johannes, J.J. Roux. 2011. "A review on phase change materials integrated in building walls". *Renewable and Sustainable Energy Reviews* 15(1): 379-391. doi: doi.org/10.1016/j.rser.2010.08.019.

Kuznik, F., J. Virgone, J. Noel. 2008. "Optimization of a phase change material wallboard for building use". *Applied Thermal Engineering* 28(11–12): 1291-1298. doi: 10.1016/j.applthermaleng. 2007.10.012.

Liu, L., D. Su, Y. Tang, G. Fang. 2016. "Thermal conductivity enhancement of phase change materials for ther-mal energy storage: A review". *Renewable and Sustainable Energy Reviews* 62: 305-317. doi: 10.1016/j.rser.2016.04.057.

Tittelein, P., S. Gibout, E. Franquet, K. Johannes, L. Zalewski, F. Kuznik, J.P. Dumas, S. Lassue, J.P. Bédécarrats, D. David. 2015. "Simulation of the thermal and energy behaviour of a compo-site material containing encapsulated-PCM: Influence of the thermodynamical modelling". *Applied Energy* 140: 269-274. doi: 10.1016/ j.apenergy.2014.11.055.

Tsilingiris, P.T. 2006. "Parametric space distribution effects of wall heat capacity and thermal re-sistance on the dynamic thermal behavior of walls and structures". *Energy and Buildings* 38(10): 1200-1211. doi: 10.1016/j.enbuild.2006. 02.007.